Original article

Exploring the effects of the curvature of the universe and the growth of Large-Scale Structure using the Atacama Cosmology Telescope and simulated Data of the Cosmic Microwave Background

Ekollu D

Submitted: February 5, 2024, Revised: version 1, May 25, 2024, version 2, May 28, 2028
Accepted: May 28, 2024

Abstract

The Data from NASA's Code for Anisotropies in the Microwave Background (CAMB) was processed with instrumental discrepancies and noise being simulated–including but not limited to - Sunyaev Zeldovich (SZ) maps, instrument beams, white noise, diffraction, and atmospheric noise, to generate a power spectrum. Subsequently, data from the Atacama Cosmology Telescope (ACT) was filtered using standard filtering techniques such as Fourier Transforms and Convolutions, among others. It was found that the resulting power spectrum from the CAMB data closely matched the power spectrum obtained from the ACT real-world data. Finally, a reverse iterative procedure was applied to a CAMB power spectrum of a universe with a curvature of 2 to generate the Cosmic Microwave Background (CMB) temperature power spectrum for such a curved universe. Analysis of the two CAMB generated temperature power spectra found significant differences between a curved and flat universe in the dark matter density, polarization spectra, and temperature. The curved universe and ACT data were used to visualize polarization in the CMB and generate polarization maps.

Keywords

Cosmic Microwave Background, Inflation theory, CMB power spectrum, Atacama cosmology telescope, Flat universe, Curved universe, Dark matter density, Polarization maps, Large Scale Structure, Anisotropy

Dhanush Ekollu, Saratoga High School, 20300 Herriman Ave, Saratoga, CA 95070, USA.
dhanush.ekollu@gmail.com

Introduction

Inflation Theory

The current standard Big Bang Theory posits gradual growth throughout the universe's lifetime (1). While this theory explains many phenomena, including the Cosmic Microwave Background's (CMB) blackbody spectrum, it is challenged by - and cannot entirely explain - The Horizon Problem, The Flatness Problem, and The Magnetic Monopole Problem. Inflation Theory solves these problems. It proposes that the universe had a short period of extreme, rapid growth following its birth; lasting from 10^{-36} seconds after the Big Bang singularity to between 10^{-33} seconds and 10^{-32} seconds after the singularity. After this period of exponential expansion, the universe subsequently expanded at a slower pace (2).

The Horizon problem

The Horizon problem is that the universe's uniform background temperature is unexpected. There was not enough time for the universe to equilibrate because the expansion would move parts of the universe away faster than the speed of light. Consequently, those parts would never have been in causal contact with each other or interact with each other to equalize to the same background temperature. Despite that, every new part of the universe seen (as their photons reach Earth for the first time) has the same properties as our part. Inflation, if it occurred, would explain this discrepancy. If the universe was very small, particles could equilibrate at that time and possess a uniform background temperature, and then the universe would expand at a more rapid rate (3).

The Flatness problem

The Flatness problem states that it is extraordinarily unlikely for the universe to be as flat as it is now–the universe would have to be at the perfect critical density and require the perfect initial conditions. Inflation solves this problem because it stretches the curvature of the universe to make it very flat (3).

The Magnetic Monopole problem

Finally, the Magnetic Monopole problem questions why no magnetic monopoles can be found, despite a considerable number of stable magnetic monopoles that should have formed in the early universe. Inflation does not rule out their existence, but it solves this problem by stating that the magnetic monopoles produced in the early universe would be pushed very far apart, and their perceived density would reduce significantly once the universe's temperature became too cool to produce new ones (4).

Large Scale Structure

Inflation also explains why Large-Scale Structures are seen today. Since there was a period of exponential expansion when the universe was born, anything not bound together expanded along with it. Small quantum fluctuations during this period of inflationary expansion were greatly amplified and gravity further exacerbated these over-densities, causing the formation of Large-Scale Structure as seen in galaxy superclusters. Thus, Inflation theory solves the three aforementioned cosmological problems, explains the presence of Large-Scale Structures, and also clarifies why a few inhomogeneities remain in the universe's density and curvature. However, Inflation is yet another theory as of now– albeit one whose assumptions can be supported with very precise measurements of the CMB (5).

The Cosmic Microwave Background

The CMB is microwave relic radiation left over from the Big Bang and is a nearly perfect blackbody (6). It is the result of an event in the universe called recombination. The CMB serves as a powerful tool to understand the initial conditions of the universe and major significant events that have occurred since its formation (Figure 1). The CMB is both a map of the universe and a timeline of its historic events. It also contains an imperative way to prove Inflation theory, solving many of the current cosmological problems that daunt cosmologists today.

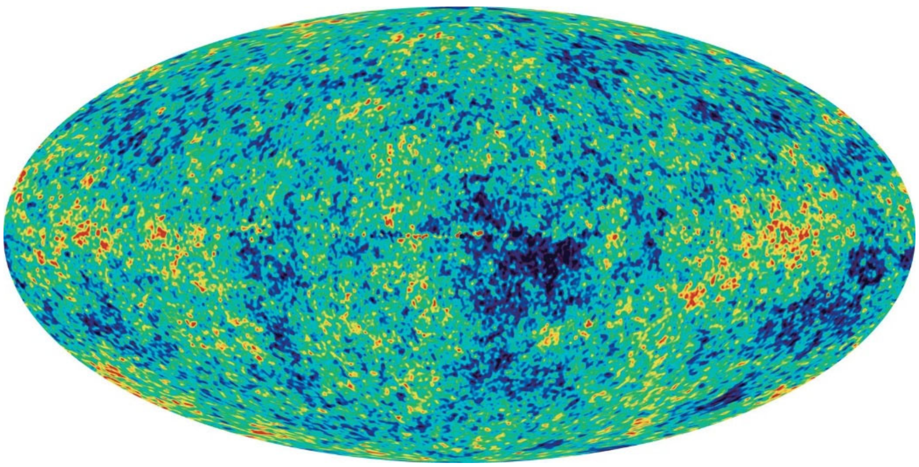

Figure 1. A full sky map of the CMB produced by the Wilkinson Microwave Anisotropy Probe (WMAP) (7).

Acoustic oscillations and the CMB's history

Prior to recombination, photons, electrons, and baryons formed a photon-baryon fluid. Free electrons glued these photons to baryons. Baryons would follow electrons and CMB photons would not travel far before Thomson Scattering off an electron because of the density and heat of the universe at that time (8). This photon-baryon plasma had pressure, supplied by the radiation itself. Just like a gas under pressure, it resisted it, eventually expanding to a larger volume than it originally was (Rarefaction), and then subsequently shrinking back to its original size (Compression). These rarefaction and compression events caused sound waves/acoustic oscillations in the CMB (9).

Going backward in time, when the universe was 1/1000th times its current size, it was a thousand times hotter. There was enough energy then to cause fission of hydrogen atoms into protons and neutrons. Going forward in time, neutral hydrogen atoms were first formed after the universe cooled down enough. This process is called recombination. Consensus estimates are that recombination occurred ~ 300,000 years after the universe's birth. The CMB was formed at this point in time. Since the universe is almost 10 billion years old, the CMB hence serves as a record of the universe since virtually its very beginning.

The Temperature Power Spectrum

The CMB contains vital information about the events that took place in the early universe, its history, and its properties. As the CMB is further analyzed, anisotropies can be observed despite its homogeneity. These temperature anisotropies directly correlate with Large-Scale Structure in the universe. There is a higher density of galaxies in hotter regions and a significantly lower density in colder regions. The first peak in the temperature spectrum contains information about the curvature of the universe (11), the second peak is related to the amount of matter in the universe (12) and the subsequent peaks, such as the third peak define the dark matter density (13) (Figure 2). Different conditions, such as the universe being matter-dominated instead of energy-dominated, change the peaks' properties (by increasing their amplitude, for example). An analysis of the temperature spectrum can hence reveal when the universe went through its different stages.

The matter density can also be found, (for example) the greater it is, the more time it takes for CMB photons/baryons before recombining, thereby shifting the damping tails to higher multipoles. Many of the same factors found in the temperature spectrum can also be found in the damping tails, hence they provide consistency checks to double-check assumptions.

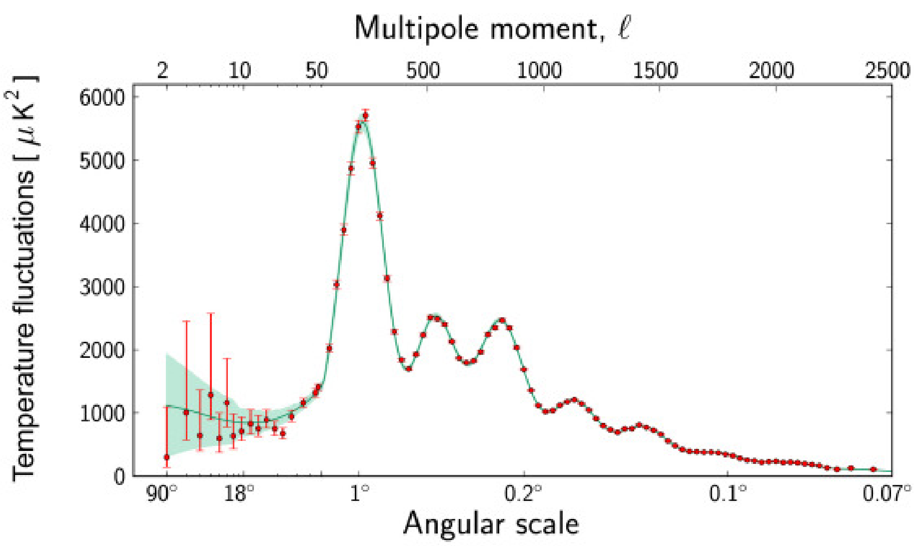

Figure 2. The CMB Temperature Power Spectrum generated by the Planck Collaboration of the European Space Agency (10).

Polarization
Unfortunately, many cosmological properties and factors cause the CMB's power spectrum to change similarly. Based on the CMB power spectrum profile alone, it is difficult to ascertain which factor or cosmological propery is responsible for the change. Fortunately, polarizations are another invaluable tool in the CMB that can be used to break this parameter degeneracy (14). They are the most direct way to investigate the conditions after recombination and later reionization. Polarizations can be differentiated into E-mode and B-mode. Commonly found E-mode polarizations (parallel/perpendicular to up/down) provide information about a majority of historic cosmic events since most cosmic events generate these type of polarizations (15). B-modes (crossed at 45-degree angles) are significantly rarer and harder to detect. These can serve as supporting evidence for Inflation theory because the gravitational waves that inflation would have caused would be expected to manifest on the CMB as B-mode polarizations (16). Figure 3 shows a representative B-mode polarization signal from the Background Imaging of Cosmic Extragalactic Polarization project (BICEP).

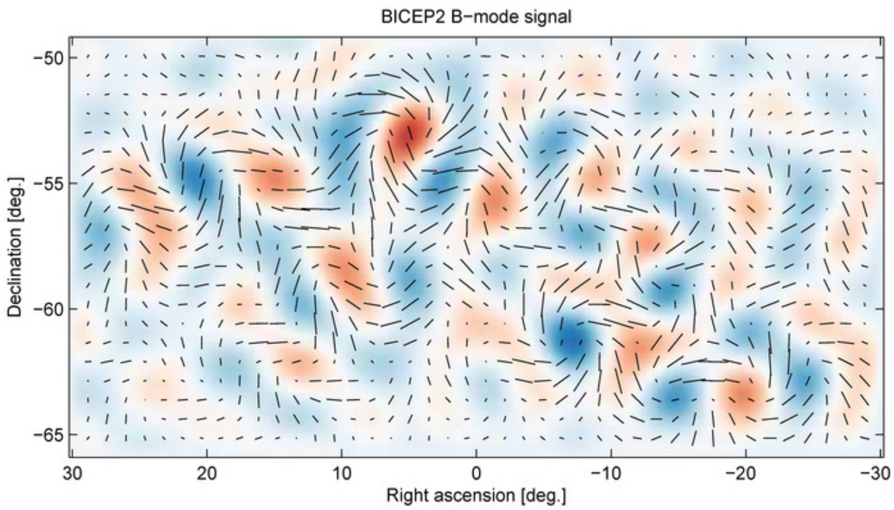

Figure 3. The B-mode signal in the CMB from BICEP2.

Results and Discussion

Notebooks prepared for the CMB Analysis Summer School held at the University of Michigan (17) were used to replicate the results. Python was used for all code. Most of the notebook's results were replicated successfully. The final code used in this paper is available at this GitHub repository: https://github.com/DEboy2007/CMBPaper.

NASA Code for Anisotropies in the Microwave Background (CAMB)

To begin, various analysis tools frequently used while working with the CMB were tested on a simulated version of our universe, in turn obtained from NASA's CAMB.

Power Spectrum

A power spectrum and temperature anisotropy map were generated for the simulated CAMB universe with the data CAMB itself provided, shown in Figures 4 and 5. The area rendered for the map was a small region of the sky made by generating a 2D power spectrum by revolving the above power spectrum; generating a Gaussian random map; multiplying the 2 maps; and using a Fourier transform to obtain the final real space map.

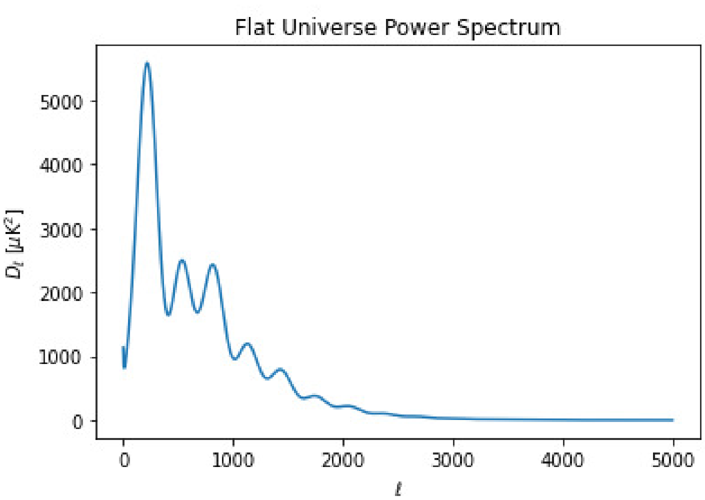

Figure 4. The angular power spectrum generated for the simulated CAMB universe, which matches the well-known and recognizable CMB power spectrum.

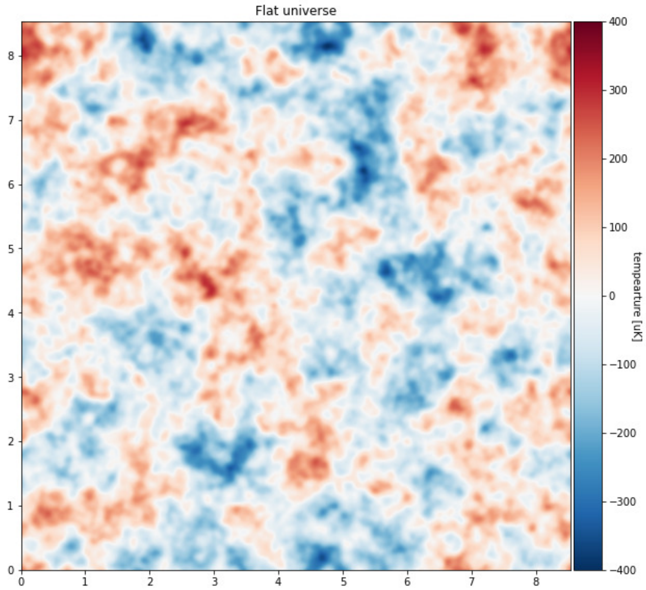

Figure 5. A temperature anisotropy map also generated from the simulated CAMB data. The area rendered was a small region of the sky made by revolving the above power spectrum, a Gaussian random map, multiplying the 2 maps, and using a Fourier transform.

Noise Maps and Completed CMB Map

The simulated map depicted in figure 5 is not realistic to what would be observed from actual telescope readings. To more realistically emulate a telescope's reading of the CMB instead of the data from NASA CAMB, the various forms of noise that usually arise while measuring data of the CMB were simulated. First, a few forms of common astrophysical noise were generated. A Point Source Map (Figure 6) was simulated–with some of the astrophysical objects approximated as a combination of faint sources and a few very bright sources. The sources were chosen to mimic a real map at 150 GHz. This frequency was chosen because the CMB peaks at 148 GHz. Point Sources are very useful for calibrating telescopes and are useful for other data analysis using the CMB, but they were subsequently filtered out for the purpose of this paper. A Sunyaev Zeldovich (SZ) map (Figure 7) was then simulated by fixing each cluster to an identical angular size. The SZ map simulation generated 500 clusters with a mean amplitude of 50, a β of 0.86, and a θ_{core} of 1.0 arcminutes. SZ maps (the Sunyev-Zeldovich effect) are a result of subtle distortions imprinted on the CMB when the dilute gas; which is at a temperature of millions of kelvin in clusters of galaxies; interacts with CMB photons to provide them with increased energy. For better simulations, a range of cluster sizes were used. Using this method, a full sky map that contained the detected CMB Anisotropies with the added noise from astrophysical noise was generated.

To account for telescope diffraction, the map from figure 7 was convolved with a Gaussian beam pattern with an FWHP = 1.25 degrees. Several types of noise were added such as white noise (10 μK-arcmin) drawn from a Gaussian distribution, atmospheric noise which grew larger on large angular scales, and 1/f noise in the detectors. White noise contains an equal amount of energy across all frequencies, while 1/f noise has more power at lower frequencies and less at higher frequencies. Atmospheric noise is noise from sources like water vapor and turbulence due to high altitude, among others. Telescopes are usually turned off when water vapor is too high due to a storm because the vapor can interfere with the microwave radiation by absorbing and re-emitting it. See Figure 8 for the instrument noise map.

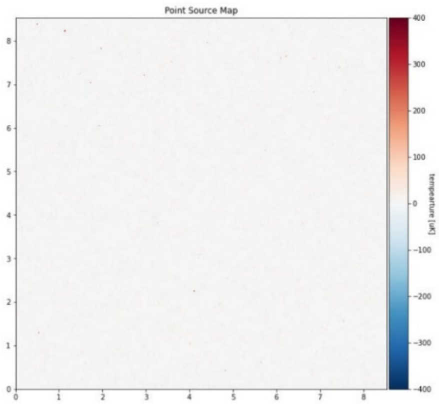

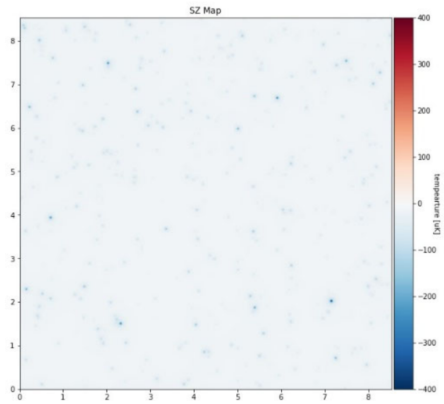

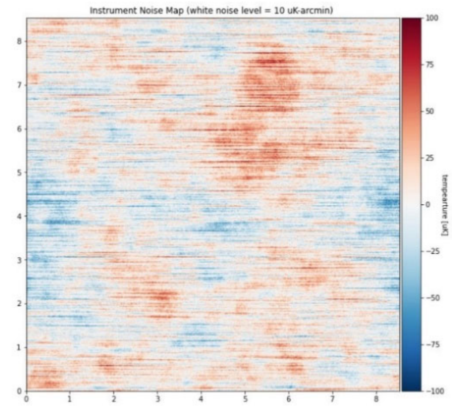

Figure 6. Point Source map (left). **Figure 7.** SZ Map (middle). **Figure 8.** Instrument noise map (right).

Finally, these noise maps and the simulated convolved sky map were added to generate a complete simulated CMB map (Figure 9) including all key astrophysical and instrumental effects. This result was fully replicated as demonstrated in the notebook (17).

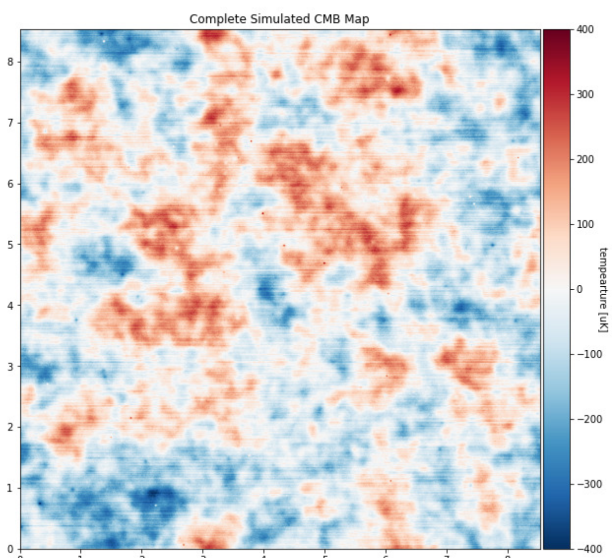

Figure 9. The complete simulated CMB sky map, with all key astrophysical and instrumental effects added to the temperature anisotropy map.

Apodizing maps

Next, the power spectrum was computed from the CMB Map, working in the same flat sky approximation (treating the celestial sphere as a flat plane for mathematical calculations and analysis) as before when the simulated CMB Map was generated. A CMB map itself is not particularly useful in understanding the nuances of astrophysical phenomena, but it is an good first tool in understanding how noise affects the interpretation of the CMB and how to mitigate its effects with the appropriate filtering tools. Once the map is filtered, it can be used to generate a power spectrum which is much more useful and amplifies the power of the CMB signal with little noise. The peaks of the power spectrum contain vital information about the universe, so it is crucial to get as accurate of a reading as possible of the CMB signal. Before undertaking a 2D Fast Fourier Transform (FFT), various windows were experimented with to apodize the map and eliminate edge effects, avoiding spurious signals. A 2D FFT is usually the obvious first step when calculating a power spectrum and is a mathematical operation that is used to transform a two-dimensional spatial domain signal or image into its frequency domain representation. Apodizing a map is where a function is used to smooth the edges of a map and filter out unwanted artifacts. A cosine window was implemented first, as shown in Figure 10.

Other windows were also experimented with, such as a sine window (Figure 11) and a sine squared window (Figure 12). These windows resulted in expected parts of the map becoming suppressed based on the nature of the functions and their graphs.

Since some of the noise in the CMB map is frequency-dependent, a high-pass filter and a filter that weights the Fourier modes by 1/A (where A is the amplitude of the noise distribution) was used to filter the noise as well.

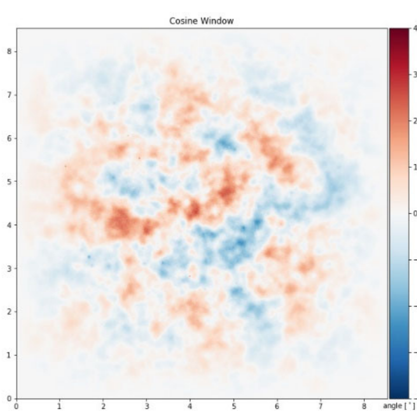

Figure 10. Apodized using cosine window.

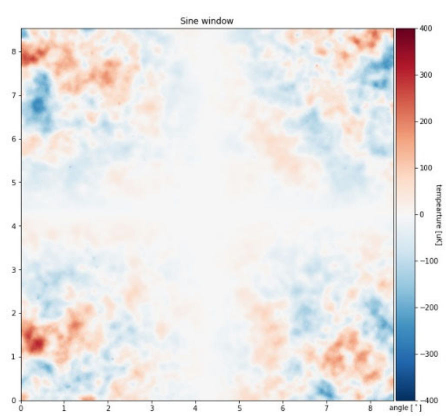

Figure 11. Apodized using sine window.

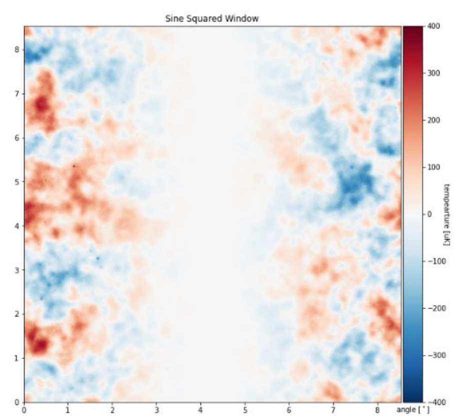

Figure 12. Apodized using sine^2 window.

Naive Power Spectrums

Next, a naive power spectrum was computed (Figure 13) and compared to the input power spectrum used for the simulations. This power spectrum was computed by applying a 2D FFT, taking the absolute value squared of the map in Fourier space, and averaging the signal in annular bins of $k = \sqrt{k_x^2 + k_y^2}$. These bins were converted to bins in l with the scaling $l = k * 2\pi$ per the flat sky approximation.

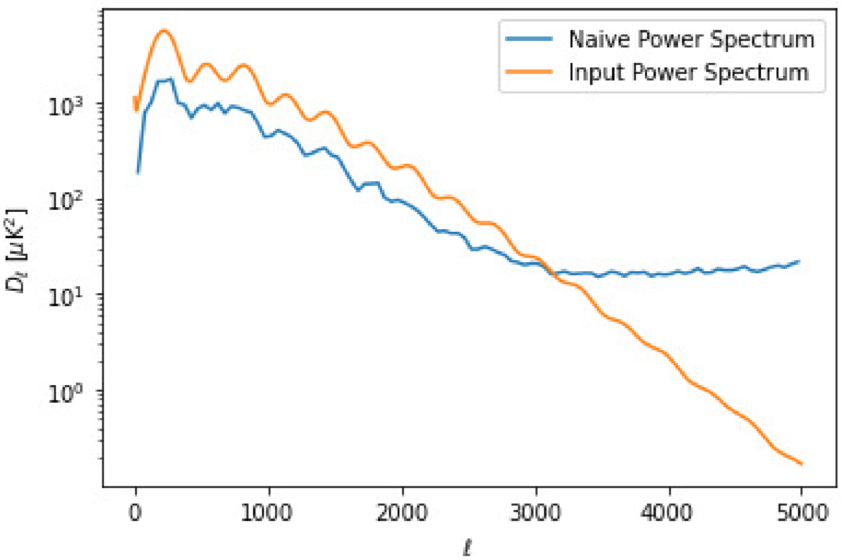

Figure 13. The naive power spectrum (blue) and the input CMB power spectrum (orange). The naive power spectrum varies due to the added instrumental and astrophysical noise such as SZ Maps and point source signals, along with suppression from the beam and apodization.

The importance of an appropriate window function is highlighted here. While window functions take away edge cases, they also lose important information about the power spectrum when the window function is too overpowering. A balance between the smoothing effects afforded by a window function and maintaining the information content of raw data is therefore crucial.

Next, the additive and multiplicative biases were corrected to get an unbiased estimate of the measured spectrum $\widehat{D}_l$ to the true spectrum D_l. $\widehat{D}_l = T * D_l + N$ The true power spectrum can be recovered with Monte Carlo techniques, using simulations to compute T (transfer function of the instrument and filtering) and N (additive noise term) and then using algebra to correct the naive measurement. This can be expressed in an equation as follows: $D_l = (\widehat{D}_l - N)/T$ The transfer function was calibrated by generating sky simulations with a known power spectrum, modeling the transfer function of the instrument and the post-processing, keeping the noise level to 0, and calculating the naive power spectrum for each simulation. Many simulations were run to reduce numerical noise and finally, the true spectrum was divided by the average signal-only spectrum to recover the estimate for the transfer function. 64 realizations were used in this example. The accuracy increased as a function of the number of realizations. This is shown in Figure 14.

The noise bias was then calibrated by running noise-only simulations through the naive power spectrum estimator and computing the average power spectrum. The error bars were computed by generating simulations including signal and noise, computing the naive power spectrum, taking the Root Mean Square of these results, and subtracting the noise bias and accounting for the transfer function. The final computed CMB Power Spectrum with error bars is shown in Figure 15.

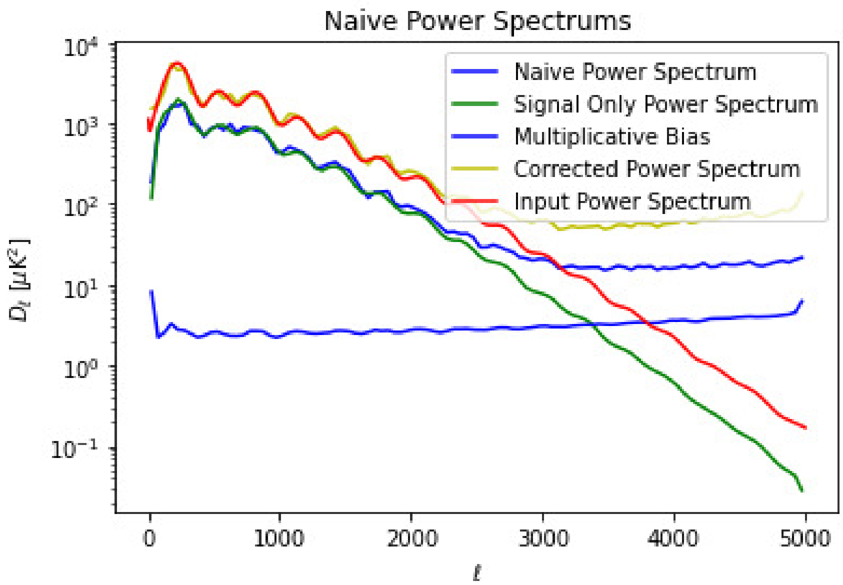

Figure 14. The estimate of the CMB power spectrum after correcting for multiplicative bias (yellow), the input power spectrum (red), the average of the signal-only simulations (green), the transfer function (blue, lower), and the naive power spectrum (blue, upper).

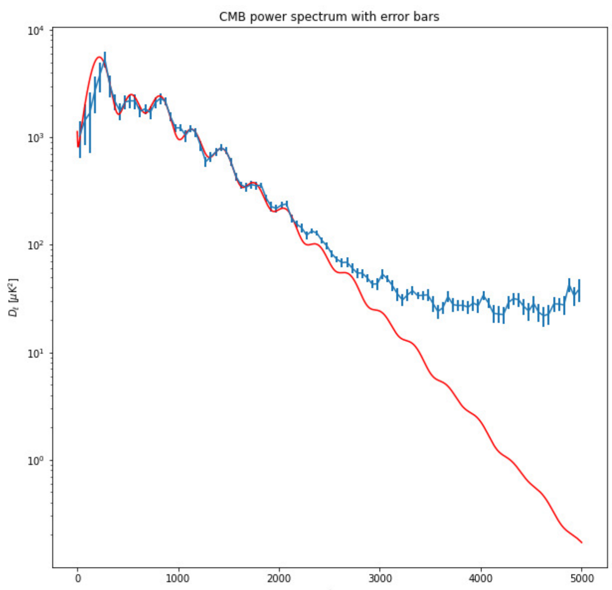

Figure 15. A computed CMB Power spectrum with error bars.

ACT Telescope Data

After sufficient testing of these tools on NASA LAMBDA CAMB, they were applied to the public telescope data from the Atacama Cosmology Telescope. To start, the public data from the Atacama Cosmology Telescope provided in the GitHub repository of the notebook was read and visualized, as shown in Figure 16.

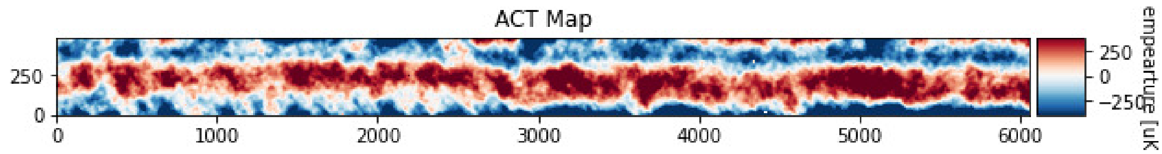

Figure 16. ACT Map - 148 GHz.

Generating maps and power spectrum

Since the ACT Map was in the form of a long stripe, 3 regions of it were cut out (in Figure 17) and the power spectrum was computed on those regions first. A cosine window was used to apodize the patches and the regions were filtered using the same techniques as with the simulated noise on the CAMB map. The filtered and apodized maps were then plotted (Figure 18). Finally, the power spectrum on the apodized maps was compared to the theoretical power spectrum, shown in Figure 19.

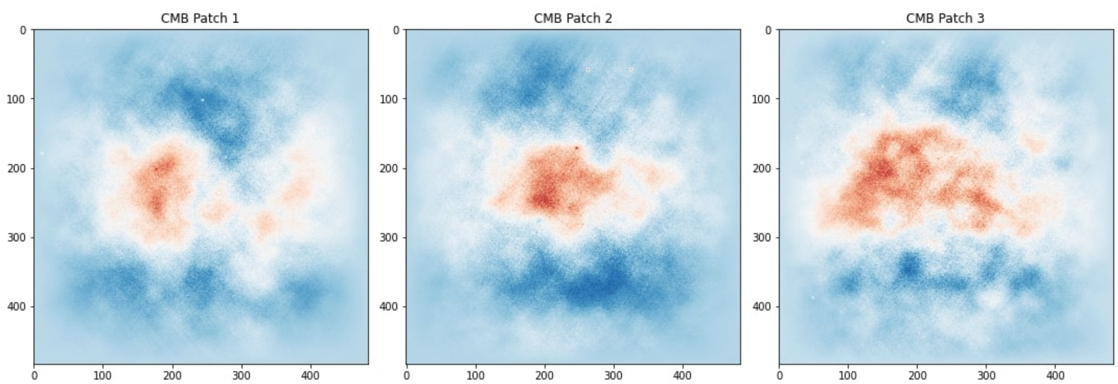

Figure 17. The three unfiltered ACT map regions.

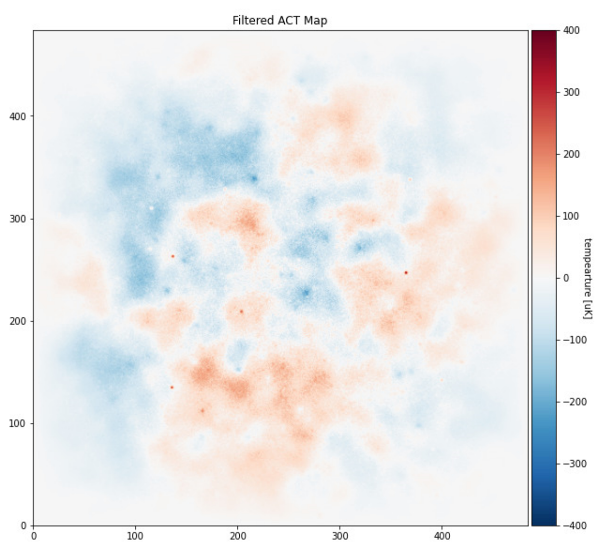

Figure 18. One of the map regions filtered.

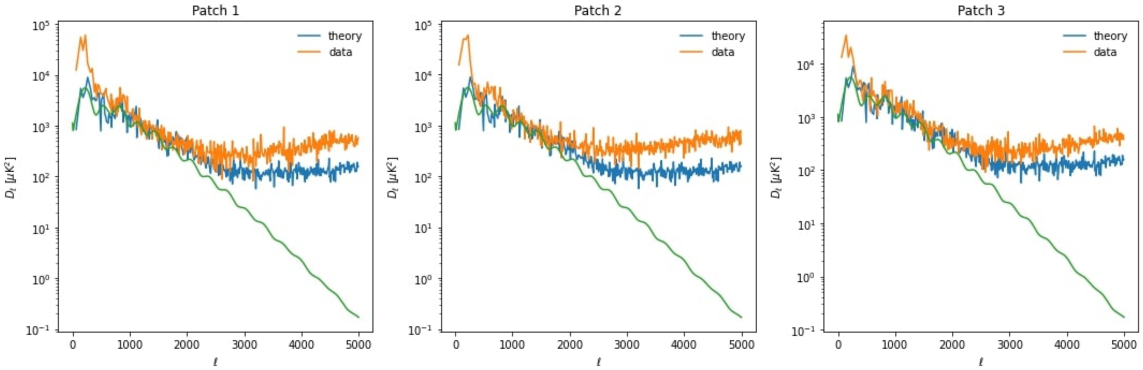

Figure 19. Power Spectrum Generated from Data vs the Theoretical Power Spectrum for each of the three regions.

The data from ACT closely matched the theoretical data in all the three regions. Both the theoretical prediction and the observed data diverged from the ideal CMB power spectrum (in green) after 2500 multipoles. Also, there is significantly more noise in the data than in the theoretical spectrum. This is because, this CMB is generated from a small region and is not the final, filtered, and analyzed version that would be published by ACT. The CMB is usually measured at various frequencies as well to take into account the atmospheric noise and subtract it effectively.

Other frequencies

The frequency dependence of maps and foregrounds was tested by analyzing ACT maps generated from the same region of the sky but at a different frequency band at 220 GHz instead of the previous 148 GHz (Figure 20). The power spectrum was calculated from that data using the aforementioned method (Figure 21).

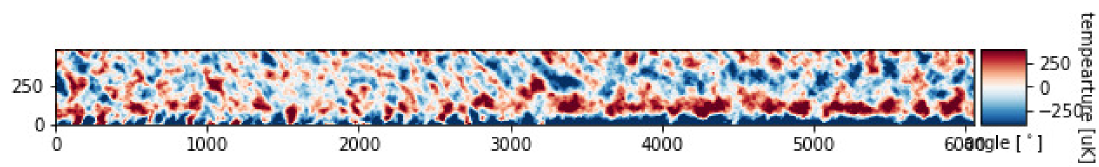

Figure 20. ACT map - 220 GHz.

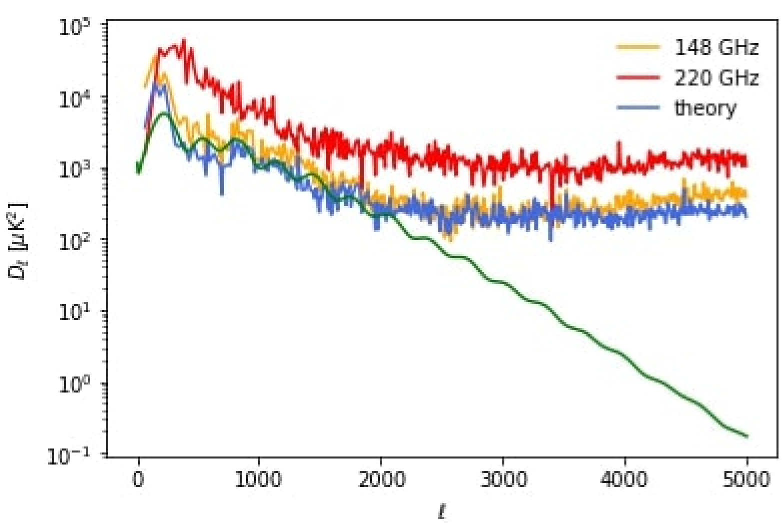

Figure 21. Power spectrum generated at 220 GHz vs the power spectrum generated at 148 GHz. The 220 GHz PS has a noise bias that is higher at all scales.

Polarizations

To begin incorporating polarizations, the code was generalized to create T, E, and B maps with the same procedure used to create T maps. T maps are temperature maps, representing the temperature fluctuations of the CMB. E maps represent the E-mode polarization of the CMB, which is curl-free. The B maps show the B-mode polarization of the CMB, which presents with swirling or twisting patterns. These maps were transformed into Stokes Q and U polarization maps and all calculations were executed in the flat sky approximation. Transforming the T, E, and B maps into Q and U maps involved a mathematical rotation that simplified the analysis and interpretation of the polarization data. The TT, EE, and BB power spectra were then plotted, shown in Figure 22 and Figure 23. A TE power spectrum, which shows the cross-correlation between the T and E power spectra, was also plotted in Figure 24.

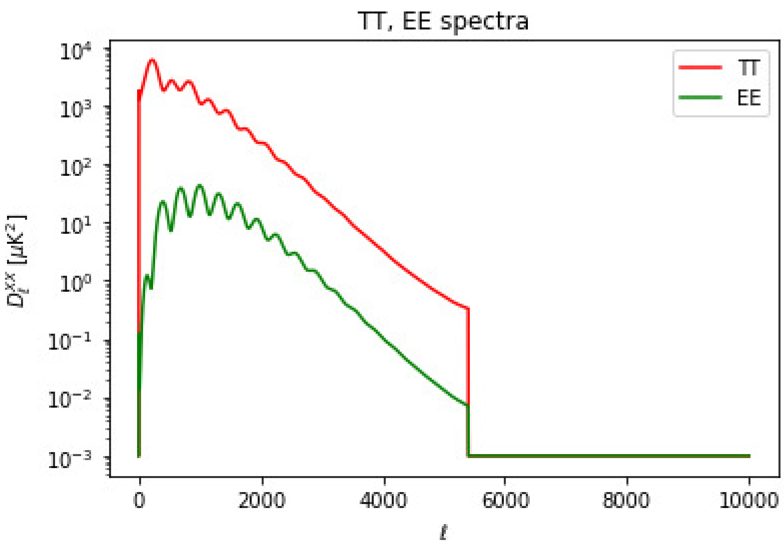

Figure 22. Plotted TT (red) and EE (green) spectra.

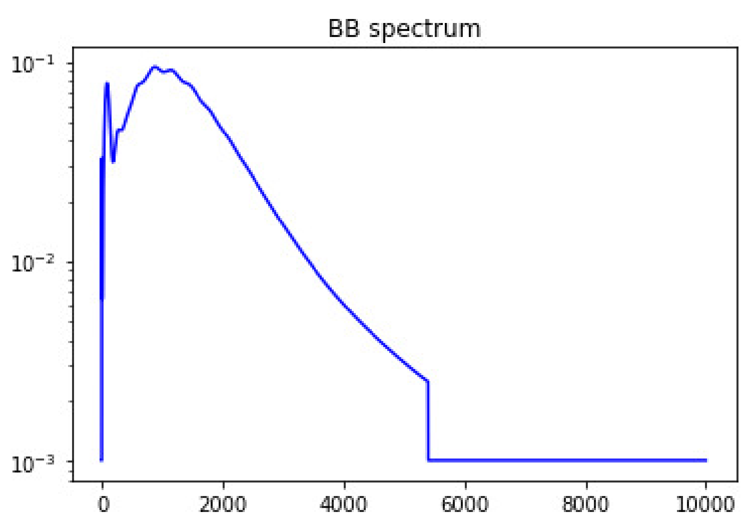

Figure 23. Plotted BB spectrum.

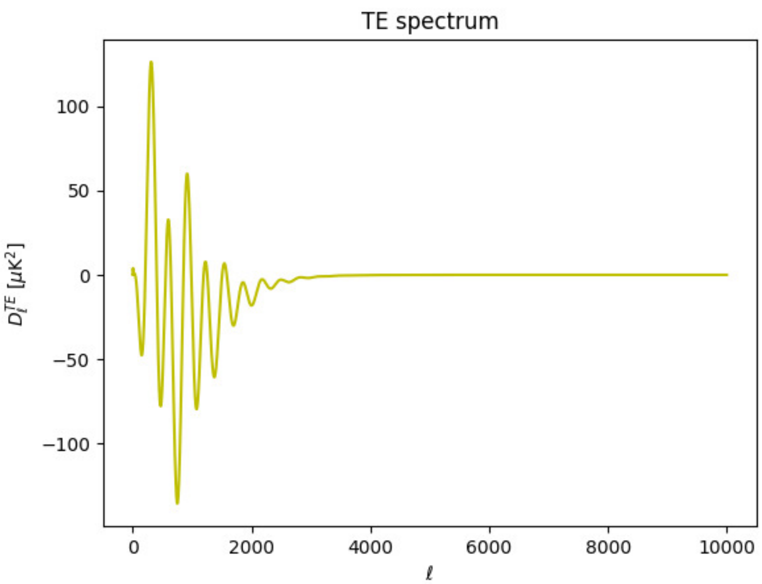

Figure 24. TE Power Spectrum, showing the cross-correlation between the Temperature and E-mode Power Spectra.

The polarization fields for E-modes can be directly visualized. The vectors were generated by visualizing the polarization field as a vector field of headless vectors that show the direction and amplitude of the linearly polarized light. A plot of vectors was generated by drawing vectors of length $p = \sqrt{Q^2 + U^2}$ and orientation ψ_p given by $2\psi_p = arctan(\frac{U}{Q})$. The polarization vectors for an E-mode-dominated field were visualized (Figure 25).

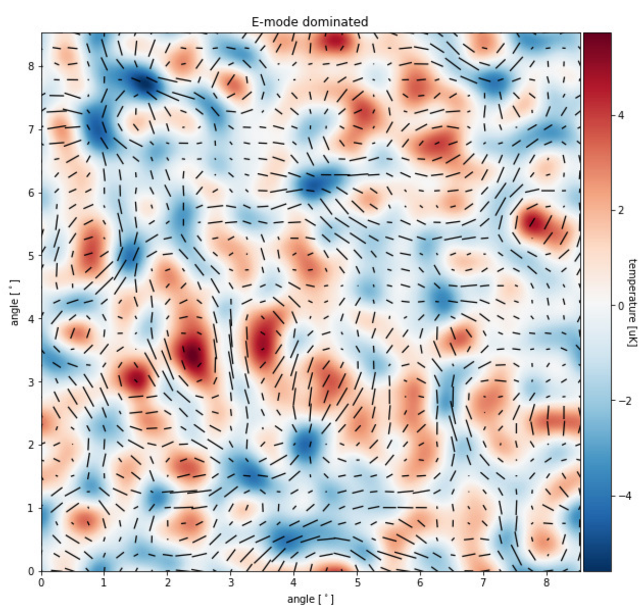

Figure 25. Direct visualization of the polarization vectors for an E-mode-dominated field. The polarization field closely traces the E-mode map.

The polarization vectors are overlayed on the map to ascertain that they closely traced the polarization around hot and cold regions. Recall that red patches are hot regions and blue patches are cold regions, and the polarization closely parallels the structure formation. There occurs an over-density of polarization where there is a formation of structure. Therefore, the behavior of polarization is closely related to cosmic structure formation. The T, E, and B maps can be simulated to show the difference between the types of polarizations. The polarization field can be visualized by both the decomposition of the CMB map into Stokes Q and U maps (Figures 26 and 27) and also E and B-modes (Figures 28 and 29). Q parameters describe the linear polarization along a reference direction, and U parameters describe the linear polarization along a direction orthogonal to the reference direction. Both E and B mode polarization can be expressed in terms of Stokes Q and U parameters:

$$E = Qcos(2\chi) + Usin(2\chi)$$
$$B = -Qsin(2\chi) + Ucos(2\chi)$$

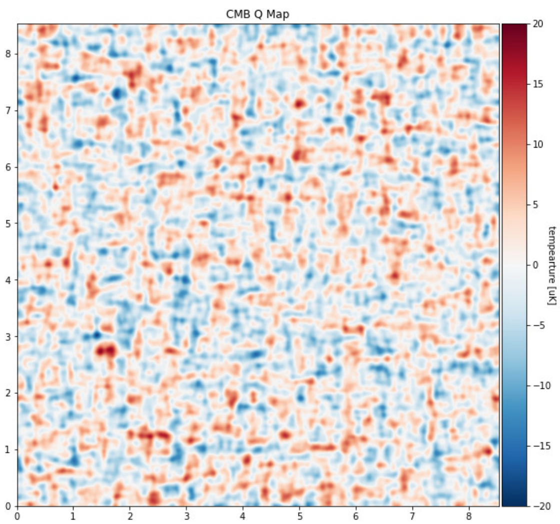

Figure 26. Q Polarization Map (left).

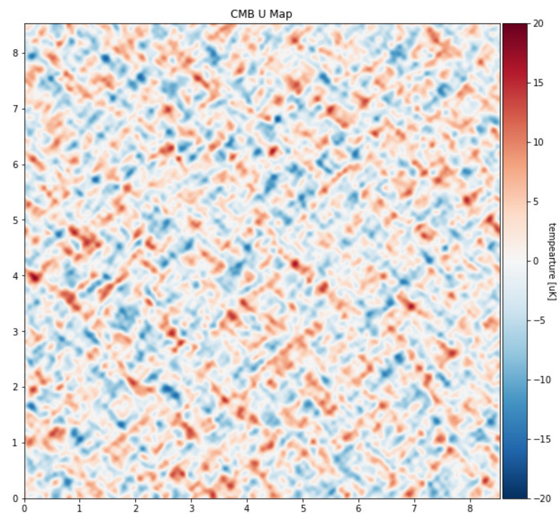

Figure 27. U Polarization Map (right).

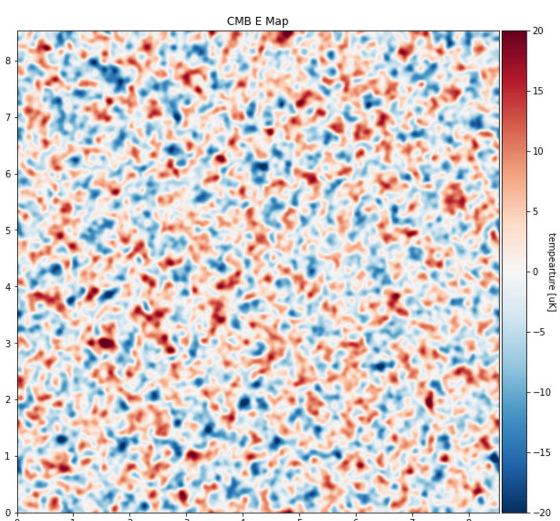

Figure 28. E Polarization Map (left).

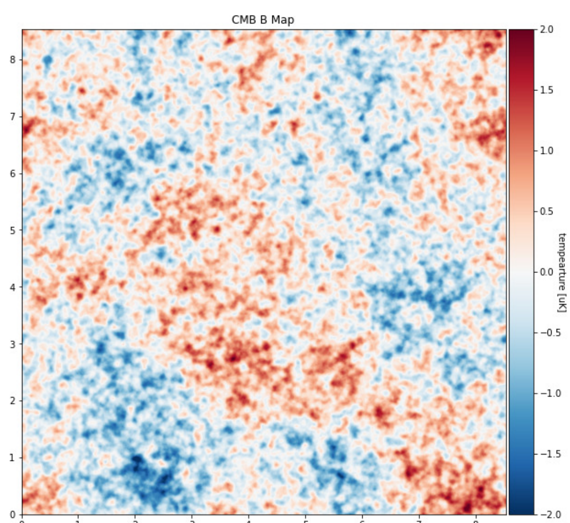

Figure 29. B Polarization Map (right).

Curved Universe

To begin, the temperature power spectra for two simulated universes–one with the same parameters as our universe and another hypothetical universe that is positively curved with an $\Omega_k = 2.0$ were generated (Figure 30). The power spectrum generated for our current flat universe correctly matched the known measured power spectrum of the CMB, shown by the blue line in Figure 30.

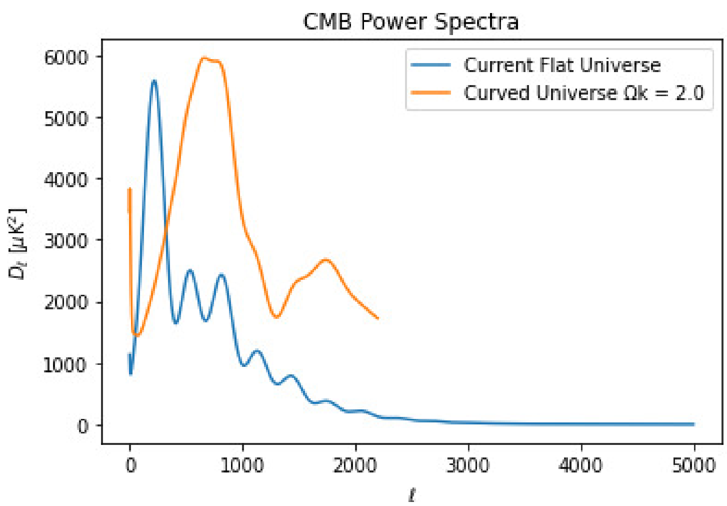

Figure 30. A comparison of the CMB power spectra of a flat universe and a positively curved universe.

As expected, the location of the first peak for the curved universe, which describes the curvature, is shifted right. Interestingly, the second peak is significantly right-shifted and there are no higher (subsequent) peaks, indicating that there is a change in dark matter density and the amount of matter in the curved universe. The curvature of the universe significantly affects the way matter in the universe is distributed and formed. There is also a noticeable dip at l=0 for the curved universe, termed the CMBR monopole. This represents the mean temperature of the CMB.

The temperature anisotropy maps for the aforementioned flat and curved simulated universes were also generated, shown in Figures 31 and 32.

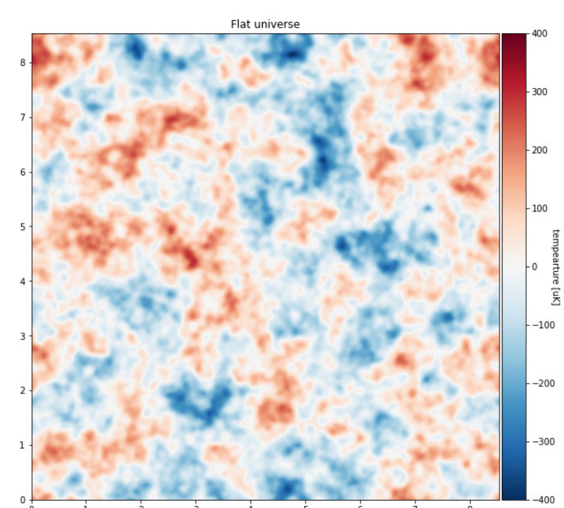

Figure 31. Temperature anisotropy map, Flat Universe (left).

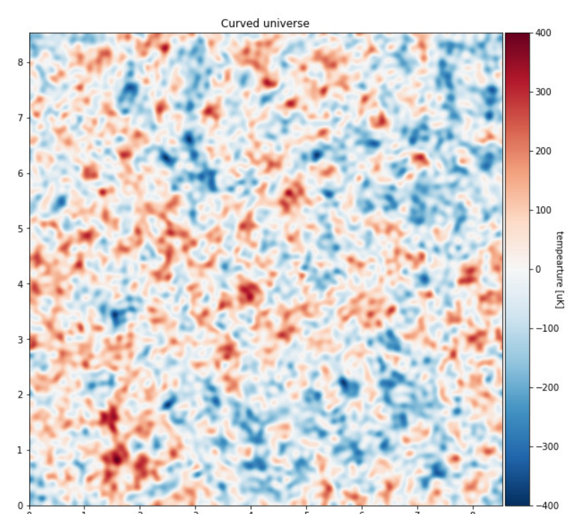

Figure 32. Temperature anisotropy map, Curved Universe (right).

Finally, the TT, EE, BB, and TE power spectra were plotted for the curved universe, shown in Figures 33, 34, and 35. The polarization spectra in a curved universe appear significantly different from their corresponding counterparts of a flat universe. The TE spectrum reaches a value of 0 faster, while the other spectra show significantly greater undulation instead of being a relatively smooth curve at higher multipoles, as in a flat universe.

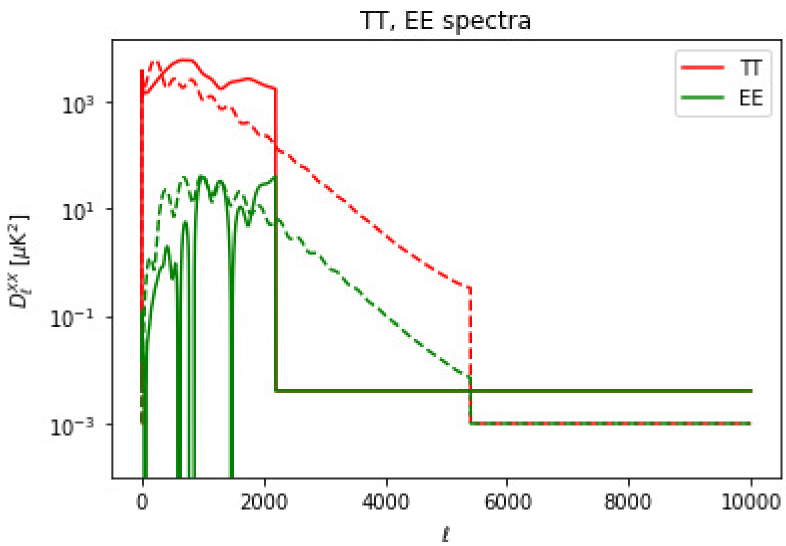

Figure 33. TT (red) and EE (green) spectra for the curved universe. The dotted lines are the previous flat universe spectra.

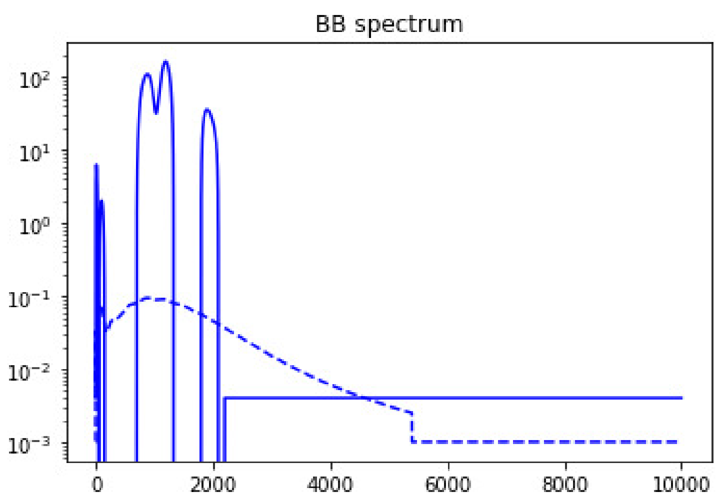

Figure 34. BB spectrum for the curved universe. The dotted line is the previous flat universe spectrum.

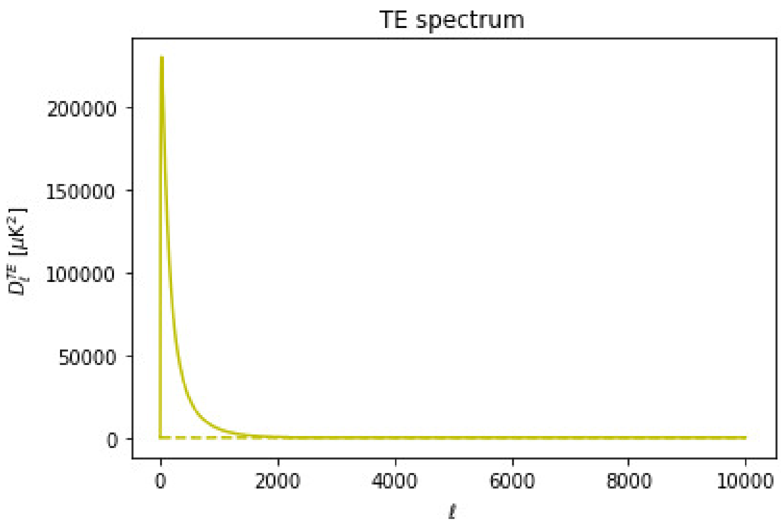

Figure 35. TE spectrum for the curved universe, showing the cross-correlation between the Temperature and E-mode Power Spectra. The dotted line is the previous flat universe spectrum.

Conclusion

In this paper, data from NASA's Code for Anisotropies in the Microwave Background (CAMB) was processed with instrumental discrepancies and noise being simulated– including but not limited to - Sunyaev Zeldovich (SZ) maps, instrument beams, white noise, diffraction, and atmospheric noise, to generate a power spectrum. Subsequently, data from the Atacama Cosmology Telescope (ACT) was filtered using standard filtering techniques such as Fourier Transforms and Convolutions, among others. It was found that the resulting power spectrum from the CAMB data closely matched the power spectrum obtained from the ACT real-world data. It was hence possible to match real-data using this particular set of simulations on the CAMB. This also suggested that the power spectrum of a universe with any other curvature could be predicted if the same set of simulations was used. The ACT telescope data was also used to generate polarization spectra and test the frequency dependence of maps. Finally, a curved universe with an $\Omega_k = 2.0$ was simulated from the CAMB data using the same instrumental discrepancies and noise as that used to generate the flat universe. Since the set of simulations remained the same, the power spectrum so obtained could be taken to be strongly suggestive of accurately depicting the curved universe, The characteristics of the curved universe's power spectrum (especially the peaks) suggested a significant change in the distribution and density of dark matter, and its polarization spectra indicated significantly different polarization. Hence, a difference in the curvature of the universe can significantly change the distribution of matter, temperature, and polarization.

References

1. Fox KC, The big bang theory: What it is, where it came from, and why it works. 2002, John Wiley & Sons, 2002, https://books.google.com.cy/books?id=_a4VmuqpZH8C

2. Sriramkumar L, An introduction to inflation and cosmological perturbation theory. Current Science, 2009, 868-886, https://doi.org/10.48550/arXiv.0904.4584

3. Guth AH, Inflationary universe: A possible solution to the horizon and flatness problems. Physical Review D, 1981, 23(2), 347, https://doi.org/10.1103/PhysRevD.23.347

4. Guth A, The magnetic monopole problem. Massachusetts Institute of Technology, Physics Department, 2018, 8, https://web.mit.edu/8.286/www/lecn18/ln09-euf18.pdf

5. Abazajian KN, Arnold K, Austermann J, Benson BA, Bischoff C, Bock J, et al. Inflation physics from the cosmic microwave background and large scale structure. Astroparticle Physics, 2015, 63, 55-65, https://doi.org/10.48550/arXiv.1309.5381

6. Durrer R, The cosmic microwave background. Cambridge University Press, 2020, https://doi.org/10.1017/9781316471524

7. Tegmark M, de Oliveira-Costa A, Hamilton AJS, High resolution foreground cleaned CMB map from WMAP. Physical Review D, 2003, 68(12), 123523, https://doi.org/10.1103/PhysRevD.68.123523

8. Sunyaev RA, The thermal history of the universe and the spectrum of relic radiation. In Symposium-International Astronomical Union, 1974, 63, 167-173, https://doi.org/10.1017/S0074180900235511

9. Bassett B, Hlozek R, Baryon acoustic oscillations. Dark energy: observational and theoretical approaches, 2010, 246, https://doi.org/10.48550/arXiv.0910.5224

10. Ade PAR, Aghanim N, Armitage-Caplan C, Arnaud M, Ashdown M, Atrio-Barandela F, et al. Planck 2013 results. XV. CMB power spectra and likelihood. Astronomy & Astrophysics, 2014, 571, https://doi.org/10.1051/0004-6361/201321591

11. Hu W, Spatial Curvature. CMB Introduction, http://background.uchicago.edu/~whu/intermediate/clcurvature.html

12. Hu W, Second Peak. CMB Introduction, http://background.uchicago.edu/~whu/intermediate/secgen.html

13. Hu W, Higher Peaks. CMB Introduction, http://background.uchicago.edu/~whu/intermediate/higher.html

14. Galli S, Wu WLK, Benabed K, Bouchet F, Crawford TM, Hivon E, Breaking the degeneracy between polarization efficiency and cosmological parameters in CMB experiments. Physical Review D, 2021, 104(2), 023518, https://doi.org/10.48550/arXiv.2102.03661

15. Henning JW, Sayre JT, Reichardt CL, Ade PAR, Anderson AJ, Austermann JE, et al. Measurements of the temperature and E-mode polarization of the CMB from 500 square degrees of SPTpol data. The Astrophysical Journal, 2018, 852(2), 97, https://doi.org/10.48550/arXiv.1707.09353.\

16. Hanson D, Hoover S, Crites A, Ade PAR, Aird KA, Austermann JE, et al. Detection of B-mode polarization in the cosmic microwave background with data from the south pole telescope. Physical Review Letters, 2013, 111(14), 141301, https://doi.org/10.48550/arXiv.1307.5830

17. jeffmcm1977, CMB Analysis Summer School. GitHub, https://github.com/jeffmcm1977/CMBAnalysis_SummerSchool